physica status solidi b
www.pss-b.com

Trap-Related Breakdown and Filamentary Conduction in Carbon Doped GaN

Christian Koller, Gregor Pobegen, Clemens Ostermaier, Gebhard Hecke, Richard Neumann, Martin Holzbauer, Gottfried Strasser, and Dionyz Pogany*

A breakdown phenomenon is studied in thin carbon doped GaN layers (GaN:C; carbon concentration $10^{19}\,cm^{-3}$) embedded between a top metal electrode and bottom n-doped GaN (n-GaN). When slowly sweeping positive bias *V* at the top electrode up and down, a hysteresis is found with transitions to on- and off-states at voltages $V_{bd,up}$ and $V_{bd,down}$ ($<V_{bd,up}$), respectively, and on- to off-current ratios exceeding 10^3. Breakdown at $V_{bd,up}$ occurs at an electric field of about $0.5\,MV\,cm^{-1}$ in GaN:C. For $V_{bd,down} < V < V_{bd,up}$, transition to on-state is time-dependent with random time-to-breakdown in the ms to 10s range. Electroluminescence measurements in on-state show conduction via multiple standing or slowly moving current filaments (CFs) which number and size increases with total current. The origin of an S-shape *I–V* curve leading to hysteresis behavior is discussed in terms of trap-related nonlinear generation-recombination processes. Formation of multiple CFs is explained by spontaneous CF formation in a homogeneous spatially extended system composed of an active medium with S-shape *I–V* curve (here GaN:C) connected in series with a passive layer (here n-GaN). Unlike previous studies in various III-N opto-electronic systems, extended defects are supposed not to be responsible for the CF origin but just for their pinning.

1. Introduction

Carbon on nitrogen site (C_N) is supposed to be a deep acceptor with the energy level 0.8 eV above the valence band maximum (E_V) of GaN causing the yellow and blue luminescence.[1,2] In AlGaN/GaN field effect transistors carbon doping compensates residual donors in GaN buffers which increases the breakdown voltage and reduces vertical leakage current.[3,4] This is supposed to be because of the Fermi-level pinning at the carbon level near E_V +0.8 eV which renders the GaN buffer semi-insulating.[5] However, negative charge trapping in the carbon-related defects causes undesirable effects such as transient decrease of drain current after returning the device from off- to on-state.[4–8] This effect is also called current collapse and is due to transient depletion of the two-dimensional electron gas.[5,8]

Recently, we have analyzed complex bias-dependent charge redistribution in thin carbon doped GaN (GaN:C) layers embedded between a top metal electrode and bottom n-doped GaN (n-GaN).[9,10] Using capacitance–voltage (*C–V*) measurements and capacitance transient spectroscopy, such a simple structure allows determining potential drops in the n-GaN and GaN:C layers both in DC and transient regimes. One of the main finding was that Fermi-level pinning at the C_N level has been confirmed.[9] At negative and moderate positive biases at the top electrode a very low leakage current has been found. At positive bias a potential barrier at the GaN:C/n-GaN interface is formed due to negatively charged carbon defects, which limits the leakage current (i.e., blocking behavior).

This work reports on the origin of a sharp current rise, referred here as "breakdown," and related hysteresis in the current–voltage (*I–V*) characteristics occurring at positive bias range not explored previously. The *I–V* measurements are correlated with electroluminescence (EL) analysis. The origin of the breakdown and observed spotty (filamentary) conduction is discussed in terms of defect-related nonlinear generation-recombination processes[11] and current filament theories for bistable systems with S-shape *I–V* characteristics.[12–14] Further the role of extended defects in the filamentation behavior is discussed. We notice that while the reverse leakage current and the blocking behavior at forward bias in the studied structures

Dr. C. Koller, Dr. G. Pobegen
KAI GmbH
Europastrasse 8, 9524 Villach, Austria
E-mail: christian.koller2@k-ai.at

Dr. C. Koller, Prof. D. Pogany
Institute of Solid State Electronics
TU Wien
Gusshausstrasse 25–25a, 1040 Vienna, Austria

Dr. C. Ostermaier, G. Hecke
Infineon Technologies Austria AG
Siemensstrasse 2, 9500 Villach, Austria

Dr. R. Neumann
Infineon Technologies AG
Am Campeon 1–15, 85579 Neubiberg, Germany

Dr. M. Holzbauer, Prof. G. Strasser
ZNMS
TU Wien
Gusshausstrasse 25–25a, 1040 Vienna, Austria

The ORCID identification number(s) for the author(s) of this article can be found under https://doi.org/10.1002/pssb.201800527.

DOI: 10.1002/pssb.201800527

can be directly related to the vertical leakage current in GaN power transistors, the breakdown phenomenon investigated here is likely not directly linked with it.

2. Experimental

Figure 1 shows schematically the investigated structures, whereby two samples with GaN:C thicknesses d of roughly 200 and 300 nm with a nominal carbon concentration of $10^{19}\,cm^{-3}$ are used. They are grown by metalorganic chemical vapor deposition on 1.7 μm thick Si-doped GaN (n-GaN) on a transition layer (TL) on 6 inch p-doped Si substrate.[9] On top of the GaN:C layers semitransparent only few nm thick Ti/Au contacts with a diameter of 220 μm are used for electroluminescence (EL) experiments and square opaque Ti/Al contacts with 100 μm side length for pure electrical characterization. The I–V and transient current measurements have been performed both in voltage- and current-controlled modes. Although I–V analysis has been performed also at various ambient temperatures, here we present only room temperature results. EL measurements have been performed from top side using a charge coupled device (CCD) image sensor and 20× microscope objective. The setup's high energy cutoff defined by optics is at 3.2 eV which is below the GaN band gap (3.4 eV).[15]

3. Results

Figure 2a,b show the typical I–V characteristics of a device recorded by sweeping positive voltage V up (solid line) and down (dashed line) with a rate of $1.5\,V\,s^{-1}$. While Figure 2a shows the data in the linear scale, (b) shows the same data in the logarithmic scale. A distinct hysteresis behavior can be seen with transition voltages $V_{bd,up}$ and $V_{bd,down}$. For $V \lesssim V_{bd,down} = 6.5$ V, further called off-state, I increases roughly exponentially with V while for $V \gtrsim V_{bd,up} = 8.5$ V, further called on-state, I increases rather linear with V with a differential resistance of $R_{diff} = 10\,k\Omega$ (see Figure 2a). I_{tr} and I_h represent trigger and holding current, respectively.

Figure 3a shows that in the off-state the current scales linearly with the device area indicating homogeneous current flow in GaN:C. The differential resistance in on-state (i.e., for $V > V_{bd,up}$, see Figure 2a) is limited by the series resistance

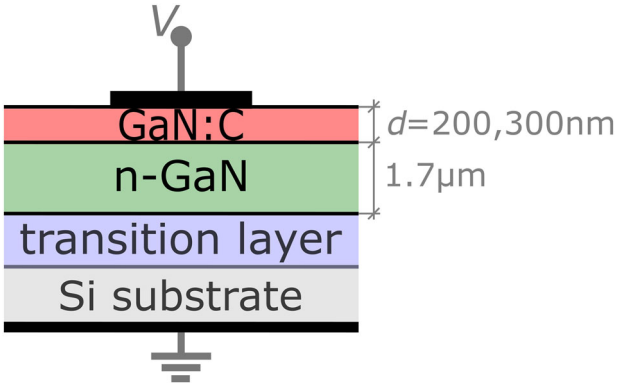

Figure 1. Schematic structure of investigated samples.

Christian Koller received the master's degree in technical physics from the Vienna University of Technology, Vienna, Austria, in 2015. He is currently pursuing the Ph.D degree in electrical engineering with the Vienna University of Technology in cooperation with Kompetenzzentrum für Automobil- und Industrieelektronik GmbH, Villach, Austria.

Dionyz Pogany received the Dipl.Ing. degree in solid-state engineering from Slovak Technical University, Bratislava, Slovakia, and the Ph.D degree from Institut National des Sciences Appliquées de Lyon, Lyon, France, in 1987 and 1994, respectively. He is with the TU Wien, Vienna, Austria, since 1995, where he is an associate professor since 2003.

of the base structure (i.e., n-GaN/TL/Si-substrate). An abrupt transition to the on-state at $V_{bd,up}$ causes current rise of 3–4 orders of magnitude. The hysteresis behavior in the bistability region $V_{bd,down} < V < V_{bd,up}$ is systematically observed over hundreds of devices on the wafer. Figure 3b compares typical up-sweep I–V curves of devices with two different thicknesses of GaN:C showing that $V_{bd,up}$ increases with GaN:C thickness.

The above results indicate the existence of an S-shape I–V characteristic with a negative differential resistance (NDR) region[12,13] which origin will be discussed later. To further investigate the bistability region we have performed measurements in current-controlled mode ("I-mode"). Figure 2c shows the I–V curves recorded in current-controlled mode sweeping the current up (thick solid line) and down (thick dashed line). The observed hysteresis in the I-mode between the trigger current I_{tr} and holding current I_h indicates more complex than just S-shape I–V curve. This is typical for spontaneous current filament (CF) formation in spatially extended homogeneous bistable systems having the S-shape current density–electric field (J–E) characteristics.[13,14,16] Thus, laterally small and large devices can exhibit different I–V curves related to respective homogeneous and inhomogeneous current flow. The introductory part of ref. [17] explains concisely the formation and branches of filamentary I–V curves.

In order to visualize the filamentary behavior, EL measurements have been performed. **Figure 4**a demonstrates homogeneous light emission in off-state which indicates homogeneous current flow at least in the μm-scale. The signal is weak requiring long integration times in the minutes range. We notice that unlike other EL measurements presented in this paper, EL in the off-state has been recorded at elevated ambient temperature (475 K) to increase the off-state current[10] and thus also the EL signal (at room temperature no signal was detected). In on-state, EL reveals the appearance of emission

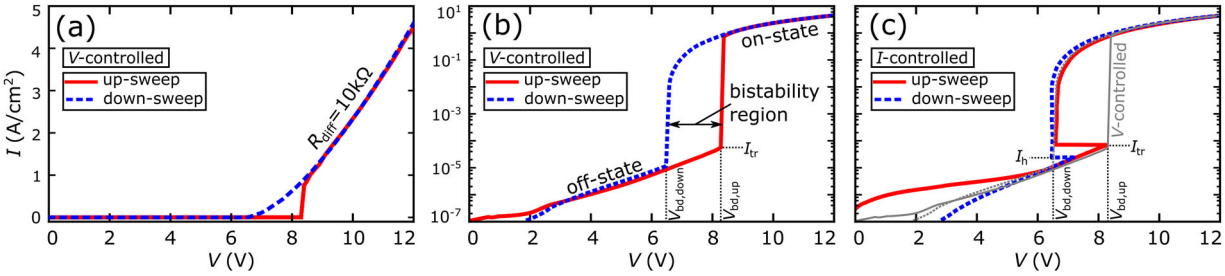

Figure 2. *I–V* characteristics for samples with $d = 200$ nm recorded in (a,b) voltage- and (c) current-controlled mode, whereby (a) shows current in linear and (b,c) in logarithmic scale. Up- and down-sweeps are represented by solid (red) and dashed (blue) lines, respectively. In (c), the voltage-controlled measurements from (a) are given by light grey lines for comparison.

spots which size and number increases with voltage or current. Each EL spot is attributed to a localized current filament (CF). Figure 4b–f show EL patterns recorded for increasing voltage. The size of a single CF grows from about 1–2 μm at 9 V up to roughly 10 μm at 20 V. Observing such a large single CF is, however, very rare since it is unstable and has the tendency to split.

The process of splitting of a larger CF into smaller multiple CFs at a constant voltage of 10 V is documented in **Figure 5**. While at the beginning (time $t = 0$) only one CF exists (Figure 5a), after 2 s it has already split into two CFs of comparable sizes (Figure 5b). At $t = 3$ s one of the new CFs has moved to the left while the first (CF1) remains pinned to the original position (Figure 5c). At $t = 5$ s the second CF has moved on to a more distant spot where its size exceeds the first spot, indicating current redistribution between the two CFs. Similar to the first spot in Figure 5a it stays rather stable until $t = 19$ s when it splits into three smaller CFs (Figure 5e). Between $t = 19$ and $t = 31$ s the three CFs on the left of Figure 5e merged again and split into two CFs as can be seen in the left part of Figure 5f. It is remarkable that the position of CF1 (see Figure 5c) remains unchanged (pinned). However, pinning for long time is rare. Some spots are more stable than others, however after a certain time they often move to different positions. It is also mentionable that by switching to off- and back to on-state CFs usually form at new positions. By recording EL videos with a time resolution of 100 ms, CFs are found to move not with a constant pace but rather jump from one metastable spot to the next within a time smaller than 100 ms and distances of few μm. The above results indicate that the number of CFs can fluctuate and that there exists a maximal stable size of a *CF*. **Figure 6** shows a typical multiple filamentary pattern at $V = 14$ V, showing that the number of CFs rises with bias or current (compare with Figure 5 for $V = 10$ V).

Up to now we have presented *I–V* measurements with a constant but slow voltage sweeping rate (Figures 2a,b and 3). By using such a method the measured parameters of the hysteresis $V_{bd,up}$ and $V_{bd,down}$ are quite reproducible from sweep to sweep. To investigate the time behavior of the transition from off- to the on-state we rapidly increased the bias from 0V to V in the bistability region, that is, $V_{bd,down} < V < V_{bd,up}$. **Figure 7** shows several such transients of current $I(t)$ recorded consecutively for $V = 9$ V for a device with $V_{bd,up} = 9.5$ V. One can see that the time-to-breakdown t_{BD} is random from case to case and varies in the ms to 10s range. As V approaches $V_{bd,up}$, the averaged t_{BD} decreases. Thus, increasing (decreasing) sweeping rate in DC measurements causes the increase (decrease) in $V_{bd,up}$ (not shown). The observed variation of breakdown time t_{BD} is likely related to the appearance of light EL spots at new positions in repeating EL measurements.

4. Discussion

The exponential rise of the current with voltage in off-state has previously been attributed to charge transport via defect bands in GaN:C whereby almost the whole potential drops in the GaN:C layer for bias $V > 1.6$ V.[9,10] Negative charge accumulation in GaN:C causes formation of a potential barrier φ_i which prevents electron injection from n-GaN into GaN:C conduction band (CB)

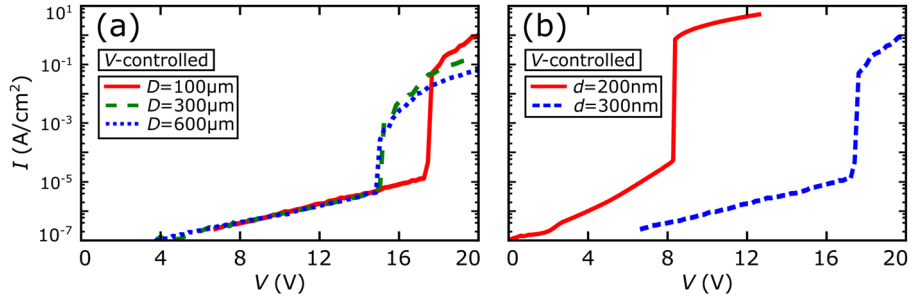

Figure 3. Voltage-controlled up-sweep *I–V* characteristics for samples with (a) different contact diameter D for $d = 300$ nm, (b) different GaN:C thickness d.

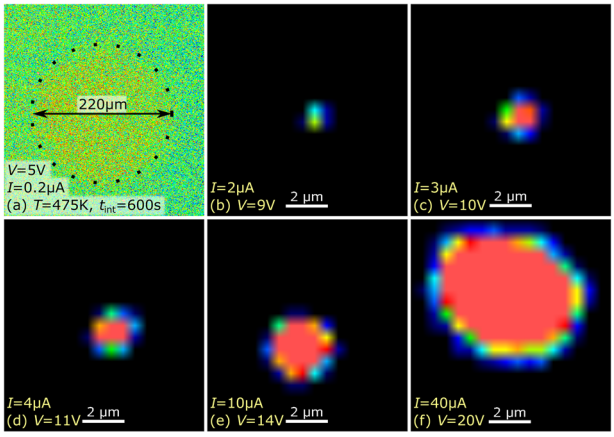

Figure 4. a) Electroluminescence image in off-state for $V = 5$ V at 475 K with integration time $t_{int} = 600$ s. Black dots represent the contact perimeter. b–f) EL images at room temperature with $t_{int} = 1$ s in on-state for different biases indicated directly in the figures. The field of view is the zoom of the active area around the position of a found EL spot. A device with $d = 200$ nm and $V_{bd,up} \approx 8$ V has been investigated.

as shown in **Figure 8**a. In the following, we consider that the sudden reduction of the height of this barrier is the origin of the breakdown.

The time-to-breakdown behavior (Figure 7) and temporal behavior of EL spots (Figures 4–6) indicate that trap-related phenomena are likely involved in the breakdown mechanism. We can exclude the self-heating effect as the reason for the breakdown initiation since the power dissipated in the homogeneous off-state produces negligible temperature rise. In literature, there exists a large class of nonlinear generation-recombination processes including defects which can lead to non-equilibrium phase transition of first order resulting in the S-shape I–V curve.[11] Considering linear potential drop in GaN:C and data of Figure 3b, the electric field at $V_{bd,up}$ is estimated to 0.4–0.5 MV cm^{-1} which is much less than the field 3–3.4 MV cm^{-1} for generation of electron-hole pairs by impact ionization in GaN.[18,19] So we can likely exclude the latter mechanism as the origin for the breakdown (here we do not consider extreme modification of electric field by strong injection effects as e.g. in

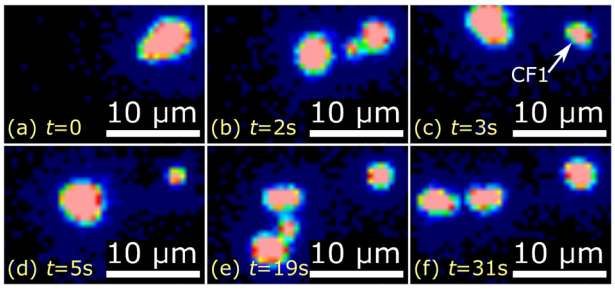

Figure 5. EL images at $V = 10$ V (averaged current = 3 μA) at six selected time instants (a–f) showing the current filament splitting, moving, and merging. The field of view is fixed around the position of EL spots. The position of a pinned filament is indicated by "CF1" in (c).

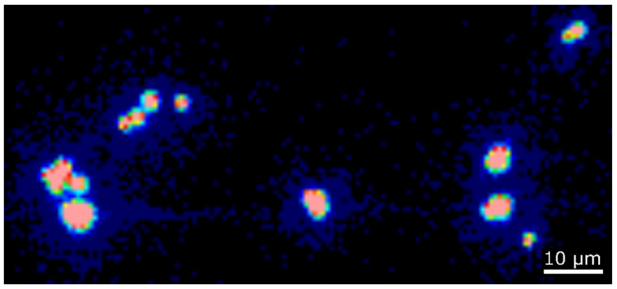

Figure 6. EL measurements recorded at $V = 14$ V (averaged current = 10 μA) showing multiple current filaments.

ref. [20]). Schöll[21] and Landsberg[22] have considered a model where the generation process governed by impurity impact ionization and the recombination process by electron-hole annihilation lead to an S-shape I–V curve. Impurity impact ionization is a kind of Auger process where a free electron from a band impinges an occupied defect state causing its ionization (see Figure 8b).[21,23] Applying to our case, when an electron injected from n-GaN into the CB of GaN:C impacts an occupied carbon defect (Figure 8c) it causes its ionization, that is its transition to non-occupied state. The resulting reduction of negative charge will decrease the potential barrier φ_i by $\Delta\varphi_i$ and thus increase the carrier injection into GaN:C (Figure 8d). This represents a closed positive feedback loop which causes the sudden increase in current at $V_{bd,up}$. The field-controlled nature of the mechanism[21,23] is consistent with our observations (Figure 3b). On the other hand, the recombination is supposed to occur between the electrons in the CB of GaN:C and holes injected from the metal contact to the valence band of GaN:C. The existence of holes is supported by the observed below band gap EL, because the unoccupied state of carbon defect required for optical transition is provided by hole capture.[1] We would like to notice that, in principle, also other trap- and field-related mechanisms can be considered leading to the NDR. Since the hole capture could also lead to the less negative trapped charge

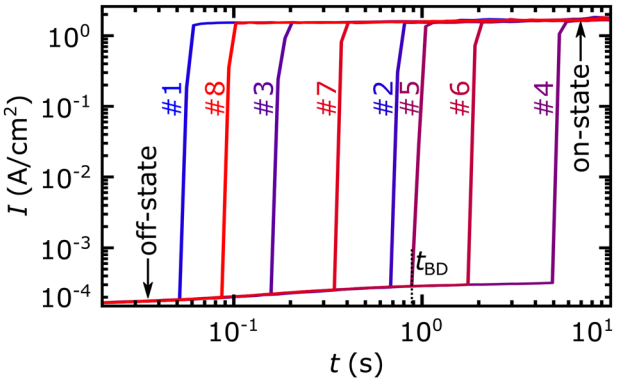

Figure 7. Current as function of time for eight consecutive measurements after bias steps from 0 to $V = 9$ V. The measurement lasted for 100 s with 10 s resting time between consecutive measurements and the number indicates the sweep number. t_{BD} indicates the time-to-breakdown for one measurement.

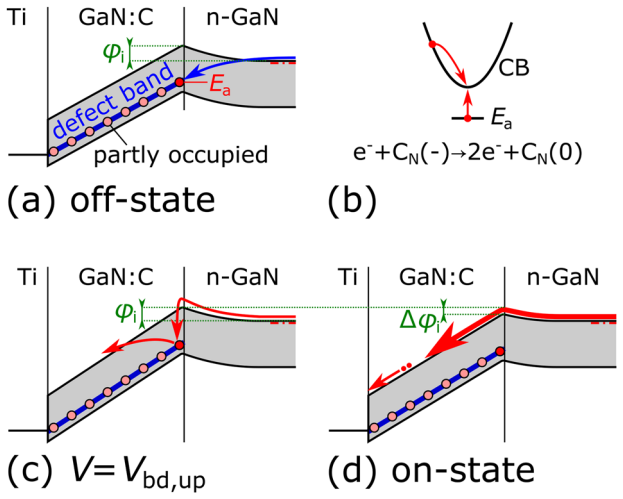

Figure 8. a) Band diagram in off-state with indicated energy position of the carbon acceptor E_a and barrier φ_i (based on ref. [9]); (b) Schematic energy – wave vector (E–k) diagram and equation representing the process of impurity impact ionization; e^- is electron, $C_N(-)$ and $C_N(0)$ the occupied and unoccupied carbon defect, respectively. c,d) are band diagrams showing the process of impurity impact ionization at the onset of the breakdown and in the on-state: (c) An electron injected from n-GaN impinges the carbon defect, (d) the ionization of the carbon defect causes less negative charge in GaN:C and thus reduces the energy barrier at the interface by $\Delta\varphi_i$. The two dots in conduction band in (d) indicate that the number of outcoming electrons is doubled (see the equation in [b]). The massive electron injection from n-GaN to GaN:C is indicated by a thick arrow.

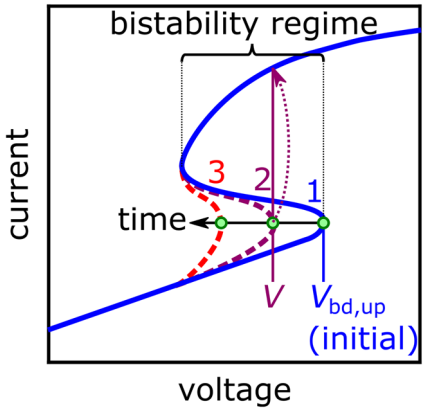

Figure 9. Schematic representation of the time evolution of the S-shape I–V characteristics: the solid line 1 is the initial I–V curve. Dashed line 2 shows the I–V characteristics at the moment of transition from off- to on-state (indicated by the dotted arrow). This occurs when the decreasing $V_{bd,up}$ reaches the applied voltage V. Dashed line 3 shows the I–V curve at later times in the on-state. The black arrow indicates the evolution of $V_{bd,up}$ with time.

and thus to the reduction of potential barrier φ_i, holes could be, in principle, also involved in the origin of the positive feedback at $V_{bd,up}$ and NDR formation. The exact mechanism still needs to be elaborated. However, self-heating effect[24] can be ruled out: considering exaggeratedly small filament size of 1 μm and typical dissipated power of 1 mW in on-state the estimated temperature rise is only few degrees which cannot explain the NDR.

We suppose that the time-to-breakdown behavior (Figure 7) is caused by the slow φ_i decrease due to slow detrapping from the carbon state, maybe also assisted by electric field.[25] The slow increase in current with time in off-state as seen in Figure 7 supports this statement. At some critically lowered barrier φ_i a positive feedback is initiated, leading to the breakdown at a local position. Phenomenologically, one can consider that the I–V curve, and the value of $V_{bd,up}$, vary with time. **Figure 9** shows the schematics of an S-shape I–V characteristic in the initial state (solid line) and at later times (dashed lines). When applying voltage V slightly below the initial $V_{bd,up}$, the shift of $V_{bd,up}$ below V will cause a sudden jump from off- to on-state (Figure 9). In summary, we consider a slow trap-related mechanism causing the time-to-breakdown behavior and a fast process of transition from off- to on-state related to an impurity impact ionization related process.

Let us discuss now the origin of multiple CFs. We consider a spatially homogeneous system with S-shape current density–voltage (J–V) characteristics. Typical $\langle J\rangle - V$ curves for small and large devices are compared in **Figure 10**a. The averaged current density $\langle J\rangle$ has been used in vertical axes so that the I–V curve with homogeneous current flow and filamentary I–V curve can be plotted in one graph. In sufficiently small devices, the current flows homogeneously and the I–V curve will have exactly the same shape as the J–V characteristics (i.e. $I = A \times J = A \times \langle J\rangle$, where A is the device area), see curve "small device" in Figure 10a. However, in a large device forced to operate in bistability region, the spatially homogeneous current flow becomes unstable against fluctuations (e.g. in carrier density and electric field).[13,14,16] As a consequence the on- and off-state regions with respective high and low current densities can eventually separate, giving rise to a CF. For extended systems where the active region with S-shape J–V characteristics is directly embedded in between two equipotential planes, the filamentary I–V characteristics shows one stable vertical I–V branch and two unstable branches,[16,17] see Figure 10a. The vertical I–V branch occurs at so-called coexistence voltage V_{co} (10 (a)), common for the whole device, where the on-state (i.e. CF) and off-state coexist. When the imposed current I increases, the size of the CF, w_F, will increase as $w_F = I/J_{co}$, where J_{co} is the current density at V_{co}, see Figure 10a. At currents greater than $\approx J_{co} \times A$ the current will flow homogeneously along the device area. The corresponding I–V part is denoted here by the "real homogeneous on-state"; the naming will be obvious later. However, in case when the active region is in series with a passive Ohmic layer (here it is the n-GaN layer), formation of multiple filaments, rather than formation of one large CF, is more favorable.[26–31] **Figure 11**a shows schematics of current flow lines in the GaN:C/n-GaN system aligned to current density distribution (b), conduction band minimum (c), and assumed charge density (d) distribution in GaN:C for such a situation. The multiple CFs are more stable due to the lateral current spreading in the Ohmic layer at the edge of the CF (Figure 11a) which causes a lower potential drop in the passive layer compared to the case of a large CF. There exists an interval of minimum and

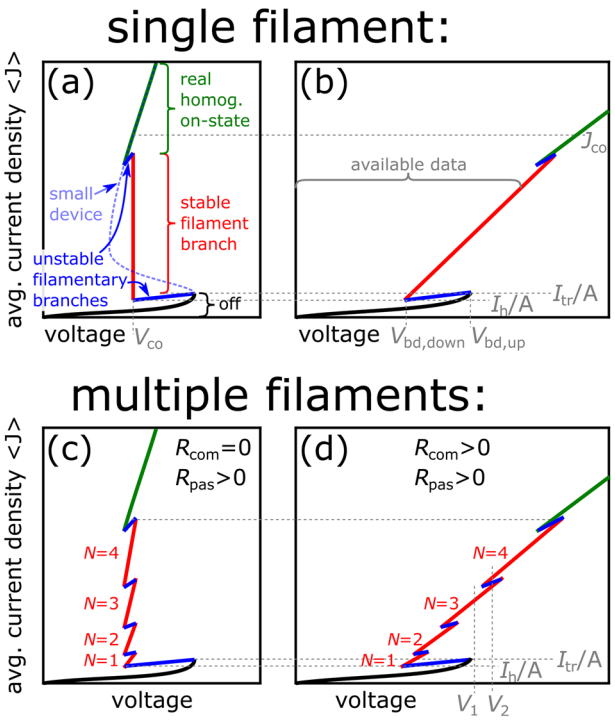

Figure 10. Schematic filamentary $\langle J\rangle - V$ curves for the cases of single (a, b) and multiple (c,d) CFs; (a,c) are the curves for $R_{com} = 0$, while (b) and (d) are for $R_{com} > 0$. The averaged current density $\langle J\rangle$ is used in vertical axes so that the I–V curves with homogeneous (see "small device" in (a)) and inhomogeneous current flow can be compared in one graph. The off-state, stable filamentary, unstable filamentary and "real homogeneous on-state" I–V branches in large devices are indicated. The voltages $V_{bd,up}$, $V_{bd,down}$ (in (b,d)) and currents I_{tr} and I_h can be directly mapped to data of Figure 2 (see mapping to "available data" range in (b)). For simplicity we consider a maximum number of four for CFs and that CFs with maximally two different NF numbers can realize. In an example in (d), at $V = V_1$ exactly three CFs are stable while at $V = V_2$ three or four CFs are stable.

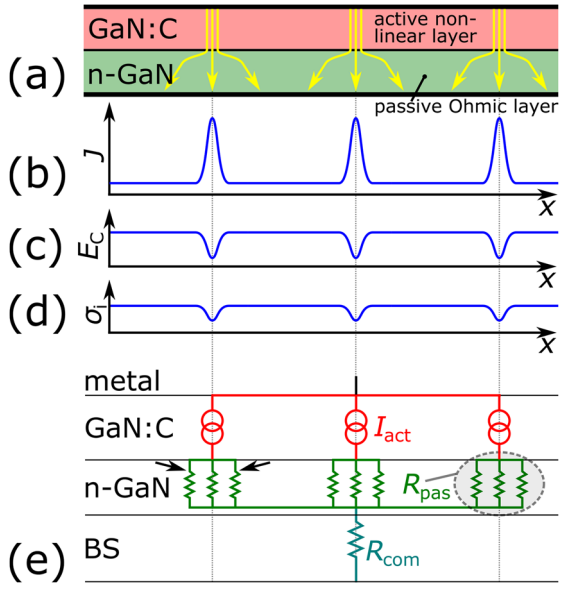

Figure 11. a) Schematic model showing current flow lines in the active GaN:C layer connected in series with a passive layer (n-GaN). In (b)–(d) the respective current density J, conduction band minimum E_c and negative charge σ_i per area in GaN:C are illustrated as function of a lateral coordinate x. e) The simplified lumped element model represents the CFs in the analyzed structure: I_{act} is a current source representing the active GaN:C, R_{pas} the resistance of the passive n-GaN layer, and R_{com} the common resistance of the n-GaN/TL/Si-substrate system called here based structure (BS). The two arrows show the parallel components of R_{pas} representing the lateral current flow in the passive layer.

maximum possible CF sizes where the CF is stable.[30] A CF with size larger than the maximum size becomes unstable and therefore splits to smaller CFs, which is also observed in our experiments (Figures 5 and 6). Within the stability interval, CFs with different numbers and sizes can appear at the same bias,[31] which is also observed in Figure 5.

A lumped element representation of the situation with multiple CFs is shown in Figure 11e, where the active element (i.e. GaN:C) represented by the current source I_{act} is connected in series with the resistance R_{pas} of the passive n-GaN layer. The resistances related to the lateral current flow are indicated by arrows in one CF. In addition, we consider a common resistance R_{com} of the base structure (i.e. n-GaN/TL/Si-substrate) system. Previously it has been shown that I–V curves related to different numbers of CFs exhibit a zig-zag behavior related to potential drop on R_{pas} due to different current flowing through a CF.[27,31] A hypothetical filamentary I–V curve for a device with a maximum number of CFs of four (NF = 4) and for $R_{com} = 0$ is shown in Figure 10c. It originates by "splitting" of the vertical filamentary branch of the I–V curve from Figure 10a when R_{pas} has a finite value. With the increase of imposed current, the averaged number of CFs increases. We notice that taking into account the observed CF diameters in the range of 3 μm, the number of CFs for our device area of 8000 μm^2 could reach several hundreds which is much larger than NF = 4.

Figure 10b,d show how the respective I–V curves from Figure 10a,c tilt when the series resistance R_{com} is considered. In Figure 10b (applicable also to Figure 10d) we indicate key parameters determining the hysteresis behavior (i.e. $V_{bd,up}$, $V_{bd,down}$, I_{tr}, and I_h), which can be directly related to the experimental data in Figure 2. One can also see that it is the tilted filamentary branch in Figure 10b,d which is mapped into the "on-state" I–V branch from experiments in Figure 2b, see the indicated "available data" range in Figure 10b. This is obvious since in our experiment we worked in the bias regime where only a part of the device area was filled with CFs, so the "real homogeneous on-state" I–V branch was not reached (see Figure 10b).

Furthermore we notice that we did not observe the zig-zag I–V behavior from Figure 10d in our data in Figure 2. We think this is due to the fact that the series resistance R_{com} is much larger than R_{pas} (see Figure 11e). As a result, we think the voltage steps related to I–V branches with different number of CFs[27,31] are very small and cannot be distinguished from noise in our experiments.

Since GaN is a material with a large concentration of extended defects such as dislocations (≈10^9 cm^{-2})[32] in the next we shortly discuss their possible role. EL spots due to localized conduction have been observed in reverse biased InGaN/GaN light emitting

diodes (LEDs).[33,34] It has been found that the EL spots occur at the position of screw and mixed dislocations,[34,35] so it is assumed that the current flows in the leakage paths related to dislocations.[32] Our results indicate that multiple CFs in the studied GaN:C/n-GaN structures are formed spontaneously. Thus, in our case extended defects are considered not to be mandatory for formation of localized CFs. However, extended defects can pin CFs at their position. The pinning observed in Figure 5 can be such a case. Pinning of spontaneously created CFs by defects has also been considered in other systems.[36] In our case, pinning can be due to local reduction in $V_{bd,up}$ caused by the charge of an extended defect (see the discussion related to Figure 9). Finally, the movement of the CFs can be caused by slight inhomogeneities in charge trapping in lateral directions which drives the CF in random directions. However, when the CF moves to the position of an extended defect, pinning can occur as mentioned above.

5. Conclusions

The observed breakdown and I–V hysteresis behavior in the studied GaN:C/n-GaN system can be attributed to a class of generation-recombination induced non-equilibrium phase transitions, leading to an S-shape I–V characteristics. When a critical electrical field is reached, the energy barrier at the GaN:C/n-GaN interface reduces which causes massive electron injection from n-GaN to conduction band of GaN:C. This is likely governed by processes of impurity impact ionization of carbon defects and electron-hole recombination, but other mechanisms leading to NDR are not excluded. The electroluminescence experiments reveal on-state conduction in form of multiple, size-limited current filaments which can spilt, merge, move, and rarely be pinned. The formation of multiple CFs is spontaneous and can be explained by theories of bistable semiconductor systems considering an active element (GaN:C) connected in series with a passive layer (n-GaN). The extended defects do not play a role in CF formation, but they can pin the CFs. The time-to-breakdown behavior is attributed to fluctuations in slow discharging of carbon defects. We also remark that in the actual EL experiments, performed at fixed voltage, the current can vary (not examined) while in EL measurements under constant current the voltage would change. Since our experiments show that the breakdown voltage $V_{bd,up}$ can evolve with time, one may expect a slightly different dynamics of CF splitting and movement under current-controlled mode.

Acknowledgements

This work was funded by the Austrian Research Promotion Agency (FFG, Project No. 863947). We thank S. Usami for valuable discussion.

Conflict of Interest

The authors declare no conflict of interest.

Keywords

carbon doped GaN, current filamentation, electroluminescence, trap-related breakdown

Received: September 29, 2018
Revised: December 7, 2018
Published online: February 19, 2019

[1] M. A. Reshchikov, H. MorkoÃ, *J. Appl. Phys.* **2005**, *97*, 061301.
[2] J. L. Lyons, A. Janotti, C. G. Van de Walle, *Phys. Rev. B* **2014**, *89*, 035204.
[3] J. Würfl, E. Bahat-Treidel, F. Brunner, M. Cho, O. Hilt, A. Knauer, P. Kotara, O. Krueger, M. Weyers, R. Zhytnytska, *ECS Trans.* **2013**, *50*, 211.
[4] M. J. Uren, M. Cäsar, M. A. Gajda, M. Kuball, *Appl. Phys. Lett.* **2014**, *104*, 263505.
[5] M. J. Uren, J. Moreke, M. Kuball, *IEEE Trans. Electron Devices* **2012**, *59*, 3327.
[6] P. B. Klein, S. C. Binari, K. Ikossi, A. E. Wickenden, D. D. Koleske, R. L. Henry, *Appl. Phys. Lett.* **2001**, *79*, 3527.
[7] A. Chini, G. Meneghesso, M. Meneghini, F. Fantini, G. Verzellesi, A. Patti, F. Iucolano, *IEEE Trans. Electron Devices* **2016**, *63*, 3473.
[8] D. Bisi, M. Meneghini, C. De Santi, A. Chini, M. Dammann, P. Bruckner, M. Mikulla, G. Meneghesso, E. Zanoni, *IEEE Trans. Electron Devices* **2013**, *60*, 3166.
[9] C. Koller, G. Pobegen, C. Ostermaier, M. Huber, D. Pogany, *Appl. Phys. Lett.* **2017**, *111*, 032106.
[10] C. Koller, G. Pobegen, C. Ostermaier, D. Pogany. In *2017 IEEE International Electron Devices Meeting (IEDM)*. **2017**, 33.4.1–33.4.4.
[11] E. Schöll, *Nonequilibrium Phase Transitions in Semiconductors: Self-Organization Induced by Generation and Recombination Processes*. Vol. *35*, Springer Science & Business Media, Switzerland **2012**.
[12] B. K. Ridley, *Proc. Phys. Soc.* **1963**, *82*, 954.
[13] E. Schöll, E. Scholl, *Nonlinear Spatio-Temporal Dynamics and Chaos in Semiconductors*. Vol. *10*, Cambridge University Press, Cambridge, UK **2001**.
[14] M. P. Shaw, V. V. Mitin, H. L. Grubin, *The Physics of Instabilities in Solid State Electron Devices*. Plenum Press, New York, London **2013**.
[15] H. Morkoc, *Nitride Semiconductors and Devices*. Vol. *32*, Springer Science & Business Media, Switzerland **2013**.
[16] A. F. Volkov, S. M. Kogan, *Sov. Phys. Uspekhi* **1969**, *11*, 881.
[17] D. Pogany, D. Johnsson, S. Bychikhin, K. Esmark, P. Rodin, M. Stecher, E. Gornik, H. Gossner, *IEEE Trans. Electron Devices* **2011**, *58*, 411.
[18] Y. Zhang, M. Sun, D. Piedra, M. Azize, X. Zhang, T. Fujishima, T. Palacios, *IEEE Electron Device Lett.* **2014**, *35*, 618.
[19] J. R. Dickerson, A. A. Allerman, B. N. Bryant, A. J. Fischer, M. P. King, M. W. Moseley, A. M. Armstrong, R. J. Kaplar, I. C. Kizilyalli, O. Aktas, J. J. Wierer, *IEEE Trans. Electron Devices* **2016**, *63*, 419.
[20] M. Levinshtein, J. Kostamovaara, S. Vainshtein, *Breakdown Phenomena in Semiconductors and Semiconductor Devices, Selected Topics in Electronics and Systems*. Vol. *36*, World Scientific Publishing, Singapore **2005**, p. 81.
[21] E. Schöll, *Proc. R. Soc. Lond. A* **1979**, *365*, 511.
[22] P. T. Landsberg, *Eur. J. Phys.* **1980**, *1*, 31.
[23] V. Sankin, A. Monakhov, P. Shkrebiy, P. Abramov, N. Sablina, N. Averkiev, *Appl. Phys. Lett.* **2010**, *97*, 262118.
[24] W. B. Smith, D. H. Pontius, P. P. Budenstein, *IEEE Trans. Electron Devices* **1973**, *20*, 731.
[25] G. Vincent, A. Chantre, D. Bois, *J. Appl. Phys.* **1979**, *50*, 5484.

[26] H.-G. Purwins, C. Radehaus, T. Dirksmeyer, R. Dohmen, R. Schmeling, H. Willebrand, *Phys. Lett. A* **1989**, *136*, 480.
[27] D. Jäger, H. Baumann, R. Symanczyk, *Phys. Lett. A* **1986**, *117*, 141.
[28] A. V. Gorbatyuk, F.-J. Niedernostheide, *Phys. Rev. B* **2002**, *65*, 245318.
[29] B. Kerner, V. V. Osipov, *Phys. Usp.* **1989**, *32*, 101.
[30] K. Mayer, R. Huebener, U. Rau, *J. Appl. Phys.* **1990**, *67*, 1412.
[31] W. Mamanee, D. Johnsson, P. Rodin, S. Bychikhin, V. Dubec, M. Stecher, E. Gornik, D. Pogany, *J. Appl. Phys.* **2009**, *105*, 084501.
[32] D. S. Li, H. Chen, H. B. Yu, H. Q. Jia, Q. Huang, *J. M. Zhou. J. Appl. Phys.* **2004**, *96*, 1111.
[33] M. Meneghini, N. Trivellin, M. Pavesi, M. Manfredi, U. Zehnder, B. Hahn, G. Meneghesso, E. Zanoni, *Appl. Phys. Lett.* **2009**, *95*, 173507.
[34] S. Usami, R. Miyagoshi, A. Tanaka, K. Nagamatsu, M. Kushimoto, M. Deki, S. Nitta, Y. Honda, H. Amano, *Phys. Status Solidi A* **2018**, *214*, 1600837.
[35] S. Usami, Y. Ando, A. Tanaka, K. Nagamatsu, M. Deki, M. Kushimoto, S. Nitta, Y. Honda, H. Amano, Y. Sugawara, Y.-Z. Yao, Y. Ishikawa, *Appl. Phys. Lett.* **2018**, *112*, 182106.
[36] A. Alekseev, S. Bose, P. Rodin, E. Schöll, *Phys. Rev. E* **1998**, *57*, 2640.